

Lower hybrid waves at the magnetosheath separatrix region

B. -B. Tang¹, W. Y. Li¹, D. B. Graham², C. Wang^{1,3}, Yu. V. Khotyaintsev², B. L. Giles⁴, P. -A. Lindqvist⁵, R. E. Ergun⁶, and J. L. Burch⁷

¹State Key Laboratory of Space Weather, National Space Science Center, Chinese Academy of Sciences, Beijing, China.

²Swedish Institute of Space Physics, Uppsala, Sweden.

³College of Earth and Planetary Sciences, University of Chinese Academy of Sciences, Beijing, China.

⁴NASA Goddard Space Flight Center, Greenbelt, Maryland, USA.

⁵KTH Royal Institute of Technology, Stockholm, Sweden.

⁶Laboratory of Atmospheric and Space Physics, University of Colorado Boulder, Boulder, Colorado, USA.

⁷Southwest Research Institute, San Antonio, Texas, USA.

Key Points:

- Lower hybrid waves are observed at the magnetosheath separatrix region in asymmetric guide-field reconnection.
- Properties of these waves are presented and compared with that at the magnetospheric side.
- These waves lead to effective cross-field particle diffusion from the magnetosheath to the reconnection exhaust.

Corresponding author: B. -B. Tang, bbtang@spaceweather.ac.cn

Abstract

Lower hybrid waves are investigated at the magnetosheath separatrix region in asymmetric guide-field reconnection by using the Magnetospheric Multiscale (MMS) mission. Three of the four MMS spacecraft observe clear wave activities around the lower hybrid frequency across the magnetosheath separatrix, where a density gradient is present. The observed waves are consistent with generation by the lower hybrid drift instability. The characteristic properties of these waves include: (1) the waves propagate toward the x-line in the spacecraft frame due to the large out-of-plane magnetic field, which is in the same direction of the diamagnetic drift of the x-line; (2) the wave potential is about 20% of the electron temperature. These drift waves effectively produce cross-field particle diffusion, enabling the transport of magnetosheath electrons into the exhaust region. The observations presented in this study indicate unique features of asymmetric guide-field reconnection.

Plain Language Summary

Magnetic reconnection is a fundamental process of explosive energy conversion in space, and one important unresolved issue during this process is how plasma waves impact the magnetic reconnection. Different types of waves have been found and investigated during reconnection, including kinetic Alfvén waves, lower hybrid waves, whistler waves, upper hybrid waves, parallel electrostatic waves. Among these waves, lower hybrid waves, taken as a basic feature of 3D asymmetric reconnection, are frequently observed at the magnetospheric side. In this study, we present new observations from the Magnetospheric Multiscale (MMS) mission, showing that the lower hybrid waves can also be found at the magnetosheath separatrix in asymmetric guide-field reconnection, which enable the cross-field particle diffusion from the magnetosheath to the exhaust. These results can help deepen our understanding of the roles of plasma waves in reconnection.

1 Introduction

Magnetic reconnection is a fundamental process in plasma physics, which rapidly converts the magnetic-field energy into plasma energy. At Earth's magnetopause, reconnection is generally asymmetric, where the magnetosheath plasma (with a weaker magnetic field and a larger plasma density) reconnects with the magnetospheric plasma (with a stronger magnetic field and a smaller plasma density), and thus the reconnection differs significantly from symmetric reconnection (e.g. the magnetotail reconnection). The quadrupolar Hall magnetic field structure can become more bipolar, and the bipolar Hall electric field tends to become monopolar (Pritchett, 2008). The stagnation point is shifted to the low density magnetospheric side of the x-line (Cassak & Shay, 2007). Electron trapping and associated parallel heating becomes asymmetric, primarily occurring on the lower density magnetospheric inflow region (Egedal et al., 2011; Graham et al., 2016). Plasma waves (including large-amplitude parallel electrostatic waves, whistler mode waves and lower hybrid waves) are identified most typically on the magnetospheric side (Wilder et al., 2019; Khotyaintsev et al., 2019). In particular, the frequently observed lower hybrid (LH) waves (Bale et al., 2002; Graham et al., 2016, 2017, 2019; Khotyaintsev et al., 2016) are taken as a basic feature of 3D asymmetric reconnection (Roytershteyn et al., 2012; Price et al., 2016; Le et al., 2017). The frequency of LH waves is found near the LH frequency ($f_{LH} \approx (f_{ce}f_{ci})^{1/2}$, where f_{ce} and f_{ci} are electron and ion cyclotron frequency). In this frequency range electrons remain approximately frozen in, while ions are almost unmagnetized. These waves are driven by lower hybrid drift instability (LHDI) at the steep density gradient or by the modified two-stream instability due to the entry of the finite gyroradius magnetosheath ions into the magnetosphere, and the energy source of instability is the cross-field current at the magnetopause (Graham et al., 2019). In reconnection, LH waves are thought to play an important role, which can contribute to

anomalous resistivity and anomalous viscosity (Davidson & Gladd, 1975; Price et al., 2016, 2017; Le et al., 2017), diffusive cross-field particle transport from the magnetosheath to the magnetospheric side (Treumann et al., 1991; Vaivads et al., 2004; Graham et al., 2017), and electron heating (Cairns & McMillan, 2005).

When a finite guide-field appears in asymmetric reconnection, the reconnection structure can be further modified. The reconnection electric field has a component parallel to the magnetic field in the vicinity of the x-line, which leads to strong electron beams. These beams are unstable for electron streaming instabilities, contributing to significant electron thermalization (Drake et al., 2003; Khotyaintsev et al., 2020). The guide field can also cause the diamagnetic drift of the x-line (Swisdak et al., 2003), and affect the shape of electron crescent distributions (Bessho et al., 2019). LH waves at the low-density magnetospheric side are reported (Graham et al., 2019; Yoo et al., 2020) as the cases revealed in other reconnection events (Le et al., 2018), and due to the presence of the guide field, the propagation of these waves can have a component along the outflow direction (Zhou et al., 2018). The imposing of the positive/negative bipolar Hall magnetic field to the guide field can enhance/reduce the out-of-plane magnetic field in the two different exhausts, leading to asymmetry of the fields and plasma in both reconnection exhausts (Mozer et al., 2008), and at the magnetosheath separatrix of the exhaust with enhanced out-of-plane magnetic fields, a density gradient is revealed due to the force balance (Fig. 5 in Mozer et al., 2008). In this study, we find clear evidence of LH waves at such a sharp density gradient across the magnetosheath separatrix in asymmetric guide-field reconnection from Magnetospheric Multiscale (MMS) mission (Burch et al., 2016). The properties of these waves are further presented and compared with that at the magnetospheric side, indicating some unique features of asymmetric guide-field reconnection.

2 Observations

We present an outbound magnetopause crossing near the subsolar point on December 21, 2017 (Fig. 1(a)), and the average separation of the four MMS spacecraft is about 30 km (Fig. 1(b)). We use magnetic field data from the fluxgate magnetometer (Russell et al., 2016), electric field data from the electric field double probes (Ergun et al., 2016; Lindqvist et al., 2016), and particle data from the fast plasma investigation (Pollock et al., 2016). This event has been used to investigate the electron two-stream instability in the reconnection exhaust (Tang et al., 2020). During this outbound magnetopause crossing, we find different MMS spacecraft observe significantly different plasma and magnetic field (Fig. 1(h) - 1(k)), where the vectors are presented in a local boundary-normal (LMN) coordinate from minimum variance analysis of \mathbf{B} ($\mathbf{L} = [-0.02, -0.41, 0.91]$, $\mathbf{M} = [-0.18, -0.90, -0.40]$ and $\mathbf{N} = [0.98, -0.17, -0.06]$ (GSE)). This can be attributed to different spacecraft trajectories during the exhaust crossing as (1) the magnetopause motion in the normal direction is very slow ($\sim 5 \text{ km s}^{-1}$) from the timing analysis of B_L (Fig. 1(h)), and (2) a relatively large tangential motion of the spacecraft relative to the x-line. By comparing the MMS observations with PIC simulations (Tang et al., 2020), MMS 4 is the closest spacecraft to the x-line as it records largest B_M (Fig. 1(i)) and lowest plasma density (Fig. 1(k)) in the exhaust region and MMS 2 is the furthestmost one. In addition, the reconnection guide field (B_g) is about 10 nT, as indicated by the solid black line in Figure 1(i), which is consistent with the direct estimation from the magnetic shear of the two inflow regions, and is about 50% of the reconnecting B_L at the sheath side. The magnetosheath separatrix observed by each spacecraft is marked by the vertical color dashed lines, which is determined by the variation of ion density, ion velocity, B_M and electric field perturbations, and these electric perturbations around the lower hybrid frequency are the focus of this study.

A zoom-in of the MMS observations at the magnetosheath separatrix is presented in Figure 2, where the variation of the magnetic field and the plasma density is identified (Figure 2(a1) and (b1)). An electric field normal to this boundary ($E_{N\perp}$) is also re-

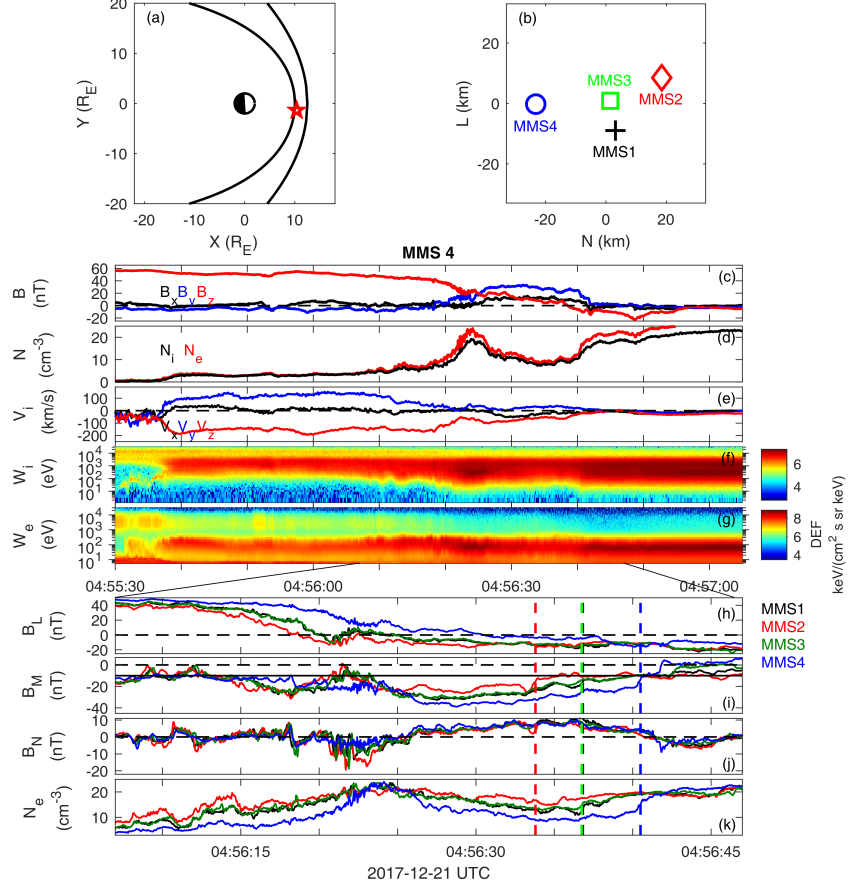


Figure 1. Overview of MMS observations at the subsolar magnetopause. (a) Equatorial projection of MMS location at 04:57 UT on 2017-12-21. (b) The relative position of MMS spacecraft. MMS 4 observations of (c) Magnetic field (\mathbf{B}). (d) Plasma number density (\mathbf{N}). (e) Ion bulk velocity (\mathbf{V}_i). (f) Ion differential energy flux. (g) Electron differential energy flux. Zoom-in of (h) B_L , (i) B_M , (j) B_N , and (k) N_e for each spacecraft. The vectors in panel (a), (c) and (e) are presented in the geocentric solar ecliptic coordinate, while other vectors are in a local boundary-normal (LMN) coordinate. The vertical color dashed lines mark the magnetosheath separatrix observed by each spacecraft, which is determined by the variation of plasma density, \mathbf{B}_M and electric perturbations.

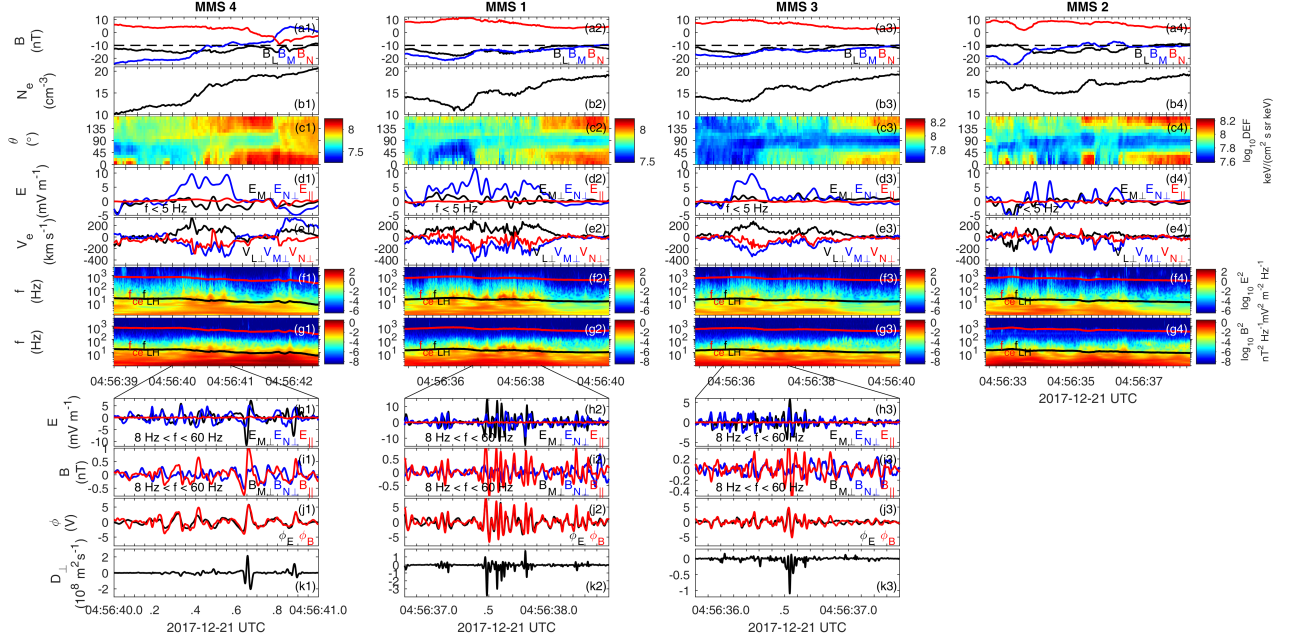


Figure 2. LH waves observed by different MMS spacecraft at magnetosheath separatrix. (a1 - k1) MMS4 observations: the magnetic field, electron number density, electron pitch angle spectrum, low frequency electric field, electron velocity, power spectral density of the electric and magnetic field, band-passing electric and magnetic field perturbations around the LH frequency, estimated wave potential (black for Φ_E and red for Φ_B) and cross-field diffusion coefficient. (a2 - k2), (a3 - k3) and (a4 - g4): The same format for MMS1, MMS3, and MMS2.

vealed, with a magnitude of 5 - 10 mV m⁻¹ (Figure 2(d1)), and similar electric field structures have also been reported in another reconnection separatrix (Yu et al., 2019), suggested to be generated by the electron pressure gradient. The power spectral density of the electric field (Figure 2(f1)) and magnetic field (Figure 2(g1)) shows enhanced perturbations near the LH frequency, which are electric perturbations perpendicular to the local magnetic field (Figure 2(h1)) and the parallel magnetic field perturbations (Figure 2(i1)). These observational features are consistent with LH waves. Similar density variations, E_{N⊥} structure and wave perturbations have been found at MMS 1 and MMS 3, but they are not obvious at MMS 2.

At lower hybrid time scales, electrons remain approximately frozen in, while ions are almost unmagnetized. If further assuming the current density perturbation $\delta\mathbf{J} = -en_e\delta\mathbf{v}_e$, the wave potential Φ_B of the LH waves can be calculated from $\delta B_{||}$ and the local plasma parameters (Norgren et al., 2012), using

$$\Phi_B = \frac{|B|}{n_e e \mu_0} \delta B_{||} \quad (1)$$

The wave potential peaks at $\sim 5 - 8$ V as shown in Figure 2(j1) (j2) and (j3). The phase velocity v_{ph} of LH waves is found by fitting $\Phi_E = \int \delta \mathbf{E} dt \cdot \mathbf{v}_{ph}$ to Φ_B . The best fitted Φ_E agrees well with Φ_B , with a correlation coefficient larger than 0.8 as listed in Table 1. The estimated phase speed is about 50 - 90 km s⁻¹ in the spacecraft frame, propagating in the -M direction and toward the x-line (+L), and the corresponding wavenumber $k\rho_e$ is about 0.9 - 1.6. The wave properties resolved from MMS 4, 1 and 3 are generally similar with each other.

Table 1. Wave properties estimated from different methods.

| MMS | $\hat{\mathbf{k}}$ (LMN) | v_{ph} (km s ⁻¹) | Φ_B (V) | Φ_E (V) | C_Φ | $k_\perp \rho_e$ | v_{ph} (km s ⁻¹) | f (Hz) | $k_\perp \rho_e$ | $\langle D_\perp \rangle$ (m ² s ⁻¹) |
|-----|-----------------------------|-----------------------------------|-----------------|-----------------|----------|------------------|-----------------------------------|------------|------------------|--|
| | Norgren et al. (2012) | | | | | | Graham et al. (2019) | | | |
| 4 | [0.62 -0.71 -0.33] | 50(58) ^a | 5.7 | 5.8 | 0.83 | 1.0 | 43(51) | 8.6(9.8) | 1.2 | $\sim 10^5$ |
| 1 | [0.72 -0.70 0.06] | 65(67) | 7.8 | 8.4 | 0.87 | 1.6 | 53(55) | 20.4(20.9) | 2.1 | -2.6×10^7 |
| 3 | [0.67 -0.72 -0.18] | 94(87) | 5.2 | 4.5 | 0.81 | 0.9 | 60(53) | 17.3(15.7) | 1.4 | -1.8×10^7 |

^a The numbers outside/inside the parentheses are estimated in the spacecraft/ion frame.

Recently, a new single-spacecraft method has been developed to determine lower hybrid wave properties (Graham et al., 2019), which is written as

$$k_\perp(\omega) = \frac{1}{d_e} \sqrt{\frac{W_e(\omega)}{W_B(\omega)}} = \frac{1}{d_e} \sqrt{\frac{W_{e,\perp}(\omega)}{W_{B,||}(\omega)}} \quad (2)$$

where d_e is the electron inertial length, and $W_e(\omega)$ and $W_B(\omega)$ are electron kinetic energy and magnetic field energy computed in the frequency domain. This method requires the sample rate of electron moments to the lower hybrid frequency, and in this study, δn_e and $\delta \mathbf{v}_{e,\perp}$ are estimated from the spacecraft potential and the measured electric field ($\delta \mathbf{v}_{e,\perp} = \delta \mathbf{E} \times \mathbf{B}/|\mathbf{B}|^2$). The top panels of Figure 3 show the dispersion relation estimated from equation (2). The characteristic frequency, wave number and wave phase speed (v_{ph}) of LH waves estimated by different MMS spacecraft are indicated by the maximum $W_E/W_{E,max}$, and the values can be found in Table 1. Overall, the computed wave properties are consistent the estimation from Norgren et al. (2012) except that the wave number is larger.

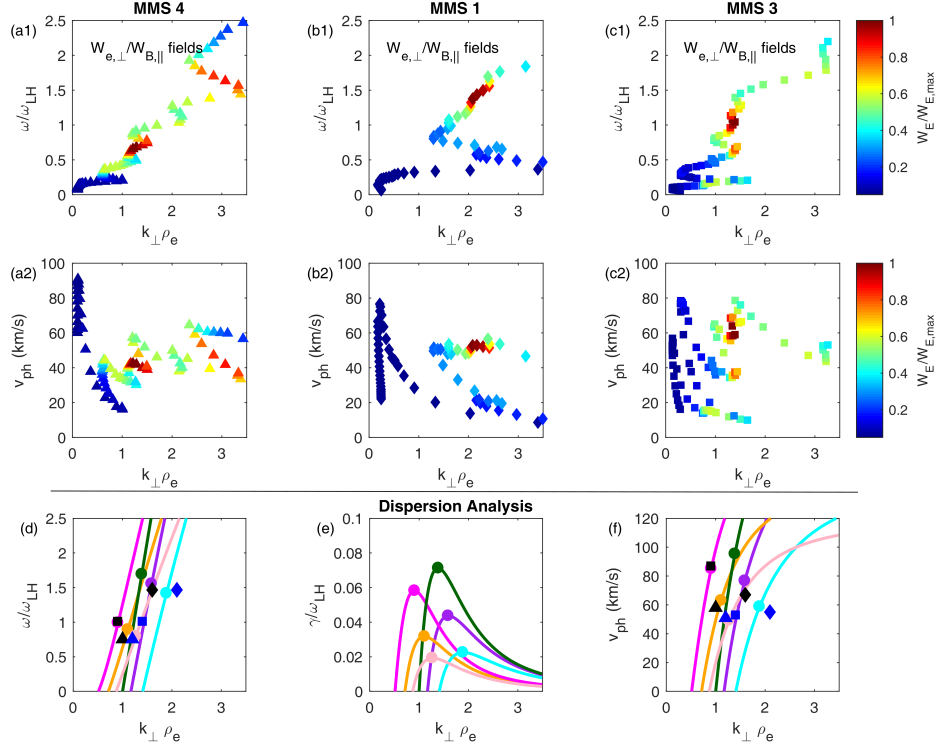


Figure 3. Dispersion of LH waves from MMS observations and theoretical analysis. (a1 - c1) Dispersion relation from different MMS spacecraft according to equation (2). (a2 - c2) Phase speed (v_{ph}) versus $k_{\perp}\rho_e$ from observations. (d - f) Frequencies, growth rates, and phase speeds versus $k_{\perp}\rho_e$ in the ion frame from the dispersion equation. The input parameters can be found in the context. The black symbols (triangle, diamond and square) are the results of different MMS spacecraft estimated from Norgren et al. (2012), while the blue ones are from Graham et al. (2019).

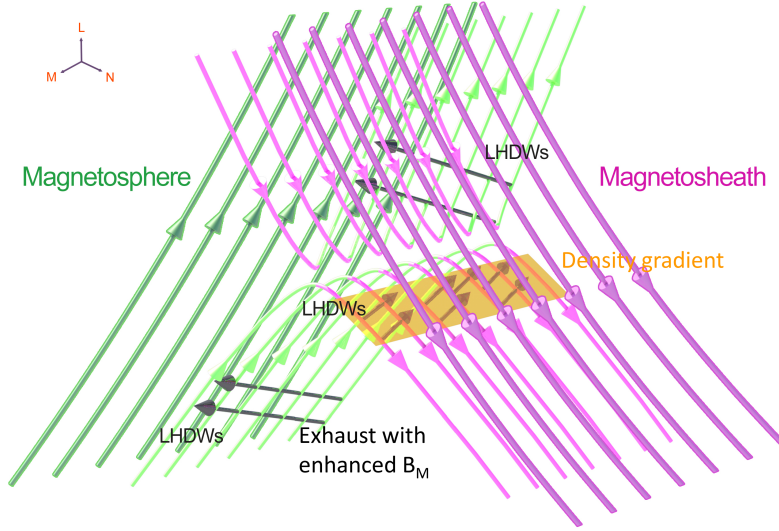


Figure 4. Schematic of LH waves in asymmetric guide-field reconnection, where the guide field is in the -M direction. The magnetosheath and magnetosphere field lines are shown in magenta and green colors. The LH waves in the local ion rest frame are indicated by the black vectors. The shaded orange region marks the density gradient at the sheath separatrix.

To investigate the instability of the observed waves, a local dispersion equation of LHDI which includes the finite plasma beta (β) effect in the ion frame is considered (Davidson et al., 1977)

$$0 = 1 - \frac{\omega_{pi}^2}{k^2 v_i^2} Z' \left(\frac{\omega}{k v_i} \right) + \frac{\omega_{pe}^2}{\Omega_{ce}^2} \left(1 + \frac{\omega_{pe}^2}{c^2 k^2} \right) + \frac{2\omega_{pe}^2}{k^2 v_e^2} \left(1 + \frac{\beta_i}{2} \right) \frac{k V_{de}}{\omega - k V_E} \quad (3)$$

where Z' is the derivative of the plasma dispersion function, $\omega_{pi,e}$ are the ion and electron plasma frequencies, $v_{i,e}$ are the ion and electron thermal speeds, Ω_{ce} is the electron cyclotron frequency, V_E is the electron drift speed due to the electric field, and V_{de} is the electron diamagnetic speed. The effect of the electron density gradient is included through V_{de} ($\mathbf{V}_{de} = -\mathbf{B} \times \nabla \cdot \mathbf{P}_e / (B^2 n_e)$). Fig 3(d) - (f) shows the predicted wave frequency, growth rate and phase speed as a function of $k_{\perp} \rho_e$. We use $B = 22$ nT, $n_e = 13$ cm $^{-3}$, $T_e = 32$ eV, $T_i = 500$ eV and $\beta_i = 5.4$, based on the observed plasma conditions. Due to the variation of the observed electron speeds at different spacecraft (Fig 2(e1)-(e3)), two groups of V_E and V_{de} are considered, which are (1) $V_{de} = 20$ km s $^{-1}$, while $V_E = 120$ km s $^{-1}$ (Pink), 150 km s $^{-1}$ (Orange) and 200 km s $^{-1}$ (Magenta); and (2) $V_{de} = 50$ km s $^{-1}$, while $V_E = 150$ km s $^{-1}$ (Cyan), 200 km s $^{-1}$ (Purple) and 250 km s $^{-1}$ (Green). For comparison, we shift the waves into the ion rest frame as shown inside the parentheses in Table 1, and we find that the ion motion is relatively small, suggesting the ion $\mathbf{E} \times \mathbf{B}$ drift is approximately balanced by the ion diamagnetic drift (Graham et al., 2019). The LH wave properties estimated by different methods (black for Norgren et al. (2012) and blue for Graham et al. (2019)) from different spacecraft (triangle, diamond and square) are also presented (Fig 3(d) and (f)), and it is shown that the waves observed at the magnetosheath separatrix are in good agreement with theoretical LHDI predictions.

3 Discussion and Summary

In this study, we have presented new MMS observations of the lower hybrid waves at the magnetosheath separatrix in asymmetric guide-field reconnection. These waves

are found to spatially coincide with the density gradient and enhanced Hall electric field across the separatrix, which is responsible for the cross-field current, the free energy source of the lower hybrid drift instability. A schematic summary of the observed LH waves is presented in Figure 4. Different with the widely observed LH waves at the magnetospheric side, the waves at the magnetosheath separatrix can only develop in limited regions where there is the density gradient. As the density gradient becomes weaker at the further downstream region, it is more difficult to allow the waves to grow. In the observation, MMS 2 does not observe clear density gradient and the wave activities around the lower hybrid frequency are not obvious. Therefore the LH waves reported in this study are less frequently to be observed than that at the magnetospheric side. Meanwhile, the density gradient revealed here is responsible to balance the enhanced out-of-plane \mathbf{B}_M in the exhaust, which could be significant when a guide field is present. So the resulting LH waves at the magnetosheath separatrix are potentially a characteristic feature for asymmetric guide-field reconnection.

The estimated wave potential of LH waves at the magnetosheath side is about 5 - 8 V, which is much smaller than the waves at the magnetospheric side (> 100 V) (Graham et al., 2019). Considering the relatively lower electron temperature (~ 32 eV), the corresponding $e\Phi/k_B T_e$ is $\sim 15\%$ - 25% , suggesting that the electrons could be effectively scattered by the wave electric field. The cross-field diffusion coefficient ($D_\perp = \delta n_e \delta v_{e,N} (\partial n_e / \partial N)^{-1}$) is shown in Figure 2(k). Throughout the wave interval, D_\perp is generally negative, corresponding to particle diffusion from the magnetosheath to the exhaust. The peak magnitude of D_\perp reaches to $\sim -3 \times 10^8 \text{ m}^2 \text{ s}^{-1}$, and the averaged value is $-1 \sim -3 \times 10^7 \text{ m}^2 \text{ s}^{-1}$ from MMS 1 and 3. The estimated D_\perp here is about one order of magnitude smaller than that at the magnetospheric side (Treumann et al., 1991; Vaivads et al., 2004; Graham et al., 2017), consisting with the relatively weaker wave perturbations, but it implies a diffusion time of several seconds over a diffusion region with its width at one wave length, which is sufficient for the broadening the density gradient across the separatrix. We note that D_\perp estimated from MMS 4 is much smaller, but the reason is not clear. Whether it is caused by the uncertainty of $\delta \mathbf{v}_e$ estimation, which does not include the electron diamagnetic drift, or by other processes still needs further investigations.

We have shown that the LH waves propagate in the -M direction and toward the x-line (+L), which is in the same direction of the $\mathbf{E} \times \mathbf{B}$ and electron diamagnetic drift direction. It is noted that the x-line is predicted to advect with the electron diamagnetic velocity (Swisdak et al., 2003), but its speed ($V_{\text{drift}} \sim (p_{e,\text{msh}} - p_{e,\text{msp}}) / \text{Ln}_e e B_g \sim 20 \text{ km s}^{-1}$, where the scale length L is approximately equal to d_i) in the spacecraft frame is smaller than the estimated LH wave phase speed. Then whether the LH waves can propagate into the x-line vicinity becomes an interesting issue. Although the LHDI has been suggested to be quenched near the x-line during antiparallel reconnection due to the large plasma beta (β) in previous studies (Roytershteyn et al., 2012; Bale et al., 2002), the oscillation of magnetic nulls has been detected to be related to the perturbations of LH waves (Xiao et al., 2007), indicating the survival of LH waves in the x-line vicinity. There are two possible explanations for this discrepancy. First, the growth rate of electrostatic LH waves is reduced by a factor $(1 + \beta/2)^{-1/2}$, if $T_e \ll T_i$ and $V_E < v_i$ (Davidson et al., 1977), meaning that LH waves would not be suppressed in reconnection with a certain guide field, in which the plasma beta is effectively reduced in the central diffusion region. Second, electromagnetic LH waves can develop in the center of a current sheet with a longer wavelength (Daughton, 2003). Overall, if LH waves can propagate into the x-line region, more investigations focusing on the dynamics related to LH waves (Chen et al., 2020) should be performed in the future.

Acknowledgments

We thank the MMS Science Data Center (<https://lasp.colorado.edu/mms/sdc/public/about/browse-wrapper/>) for providing high-quality data for this study. This work was supported by

the National Natural Science Foundation of China (grants 41974196, 41974170 and 41731070), the Chinese Academy of Sciences (QYZDJ-SSW-JSC028, XDA15052500, XDA17010301 and XDB 41000000) and the Specialized Research Fund for State Key Laboratories of China. B.-B. T. was also supported by the Youth Innovation Promotion Association of the Chinese Academy of Sciences.

References

- Bale, S., Mozer, F., & Phan, T. (2002). Observation of lower hybrid drift instability in the diffusion region at a reconnecting magnetopause. *Geophysical research letters*, 29(24), 33–1.
- Bessho, N., Chen, L.-J., Wang, S., & Hesse, M. (2019). Effects of the guide field on electron distribution functions in the diffusion region of asymmetric reconnection. *Physics of Plasmas*, 26(8), 082310.
- Burch, J., Torbert, R., Phan, T., Chen, L.-J., Moore, T., Ergun, R., ... others (2016). Electron-scale measurements of magnetic reconnection in space. *Science*, 352(6290), aaf2939.
- Cairns, I. H., & McMillan, B. (2005). Electron acceleration by lower hybrid waves in magnetic reconnection regions. *Physics of plasmas*, 12(10), 102110.
- Cassak, P., & Shay, M. (2007). Scaling of asymmetric magnetic reconnection: General theory and collisional simulations. *Physics of Plasmas*, 14(10), 102114.
- Chen, L.-J., Wang, S., Le Contel, O., Rager, A., Hesse, M., Drake, J., ... Avanov, L. (2020, Jul). Lower-hybrid drift waves driving electron nongyrotropic heating and vortical flows in a magnetic reconnection layer. *Phys. Rev. Lett.*, 125, 025103. Retrieved from <https://link.aps.org/doi/10.1103/PhysRevLett.125.025103> doi: 10.1103/PhysRevLett.125.025103
- Daughton, W. (2003). Electromagnetic properties of the lower-hybrid drift instability in a thin current sheet. *Physics of Plasmas*, 10(8), 3103–3119.
- Davidson, R., & Gladd, N. (1975). Anomalous transport properties associated with the lower-hybrid-drift instability. *The Physics of Fluids*, 18(10), 1327–1335.
- Davidson, R., Gladd, N., Wu, C., & Huba, J. (1977). Effects of finite plasma beta on the lower-hybrid-drift instability. *The Physics of Fluids*, 20(2), 301–310.
- Drake, J., Swisdak, M., Cattell, C., Shay, M., Rogers, B., & Zeiler, A. (2003). Formation of electron holes and particle energization during magnetic reconnection. *Science*, 299(5608), 873–877.
- Egedal, J., Le, A., Pritchett, P., & Daughton, W. (2011). Electron dynamics in two-dimensional asymmetric anti-parallel reconnection. *Physics of Plasmas*, 18(10), 102901.
- Ergun, R., Tucker, S., Westfall, J., Goodrich, K., Malaspina, D., Summers, D., ... others (2016). The axial double probe and fields signal processing for the mms mission. *Space Science Reviews*, 199(1-4), 167–188.
- Graham, D., Khotyaintsev, Y. V., Norgren, C., Vaivads, A., Andre, M., Drake, J., ... others (2019). Universality of lower hybrid waves at earth's magnetopause. *Journal of Geophysical Research: Space Physics*.
- Graham, D., Khotyaintsev, Y. V., Norgren, C., Vaivads, A., André, M., Lindqvist, P.-A., ... others (2016). Electron currents and heating in the ion diffusion region of asymmetric reconnection. *Geophysical Research Letters*, 43(10), 4691–4700.
- Graham, D., Khotyaintsev, Y. V., Norgren, C., Vaivads, A., André, M., Toledo-Redondo, S., ... others (2017). Lower hybrid waves in the ion diffusion and magnetospheric inflow regions. *Journal of Geophysical Research: Space Physics*, 122(1), 517–533.
- Khotyaintsev, Y. V., Graham, D., Norgren, C., Eriksson, E., Li, W., Johlander, A., ... others (2016). Electron jet of asymmetric reconnection. *Geophysical Research Letters*, 43(11), 5571–5580.

- Khotyaintsev, Y. V., Graham, D., Steinvall, K., Alm, L., Vaivads, A., Johlander, A., ... others (2020). Electron heating by debye-scale turbulence in guide-field reconnection. *Physical Review Letters*, 124(4), 045101.
- Khotyaintsev, Y. V., Graham, D. B., Norgren, C., & Vaivads, A. (2019). Collisionless magnetic reconnection and waves: Progress review. *Frontiers in Astronomy and Space Sciences*, 6, 70.
- Le, A., Daughton, W., Chen, L.-J., & Egedal, J. (2017). Enhanced electron mixing and heating in 3-d asymmetric reconnection at the earth's magnetopause. *Geophysical Research Letters*, 44(5), 2096–2104.
- Le, A., Daughton, W., Ohia, O., Chen, L.-J., Liu, Y.-H., Wang, S., ... Bird, R. (2018). Drift turbulence, particle transport, and anomalous dissipation at the reconnecting magnetopause. *Physics of Plasmas*, 25(6), 062103.
- Lindqvist, P.-A., Olsson, G., Torbert, R., King, B., Granoff, M., Rau, D., ... others (2016). The spin-plane double probe electric field instrument for mms. *Space Science Reviews*, 199(1-4), 137–165.
- Mozer, F., Pritchett, P., Bonnell, J., Sundkvist, D., & Chang, M. (2008). Observations and simulations of asymmetric magnetic field reconnection. *Journal of Geophysical Research: Space Physics*, 113(A1).
- Norgren, C., Vaivads, A., Khotyaintsev, Y. V., & André, M. (2012). Lower hybrid drift waves: Space observations. *Physical review letters*, 109(5), 055001.
- Pollock, C., Moore, T., Jacques, A., Burch, J., Gliese, U., Saito, Y., ... others (2016). Fast plasma investigation for magnetospheric multiscale. *Space Science Reviews*, 199(1-4), 331–406.
- Price, L., Swisdak, M., Drake, J., Burch, J., Cassak, P., & Ergun, R. (2017). Turbulence in three-dimensional simulations of magnetopause reconnection. *Journal of Geophysical Research: Space Physics*, 122(11), 11–086.
- Price, L., Swisdak, M., Drake, J. F., Cassak, P., Dahlin, J., & Ergun, R. (2016). The effects of turbulence on three-dimensional magnetic reconnection at the magnetopause. *Geophysical Research Letters*, 43(12), 6020–6027.
- Pritchett, P. (2008). Collisionless magnetic reconnection in an asymmetric current sheet. *Journal of Geophysical Research: Space Physics*, 113(A6).
- Roytershteyn, V., Daughton, W., Karimabadi, H., & Mozer, F. (2012). Influence of the lower-hybrid drift instability on magnetic reconnection in asymmetric configurations. *Physical review letters*, 108(18), 185001.
- Russell, C., Anderson, B., Baumjohann, W., Bromund, K., Dearborn, D., Fischer, D., ... others (2016). The magnetospheric multiscale magnetometers. *Space Science Reviews*, 199(1-4), 189–256.
- Swisdak, M., Rogers, B., Drake, J., & Shay, M. (2003). Diamagnetic suppression of component magnetic reconnection at the magnetopause. *Journal of Geophysical Research: Space Physics*, 108(A5).
- Tang, B., Li, W., Le, A., Graham, D., Wu, Y., Wang, C., ... others (2020). Electron mixing and isotropization in the exhaust of asymmetric magnetic reconnection with a guide field. *Geophysical Research Letters*, e2020GL087159.
- Treumann, R., LaBelle, J., & Pottellette, R. (1991). Plasma diffusion at the magnetopause: The case of lower hybrid drift waves. *Journal of Geophysical Research: Space Physics*, 96(A9), 16009–16013.
- Vaivads, A., André, M., Buchert, S., Wahlund, J.-E., Fazakerley, A., & Cornilleau-Wehrin, N. (2004). Cluster observations of lower hybrid turbulence within thin layers at the magnetopause. *Geophysical research letters*, 31(3).
- Wilder, F., Ergun, R., Hoilijoki, S., Webster, J., Argall, M., Ahmadi, N., ... others (2019). A survey of plasma waves appearing near dayside magnetopause electron diffusion region events. *Journal of Geophysical Research: Space Physics*.
- Xiao, C., Wang, X., Pu, Z., Ma, Z., Zhao, H., Zhou, G., ... others (2007). Satellite observations of separator-line geometry of three-dimensional magnetic reconnection. *Nature Physics*, 3(9), 609–613.

- 341 Yoo, J., Ji, J.-Y., Ambat, M. V., Wang, S., Ji, H., Lo, J., ... others (2020). Lower
342 hybrid drift waves during guide field reconnection.
- 343 Yu, X., Wang, R., Lu, Q., Russell, C. T., & Wang, S. (2019). Nonideal electric
344 field observed in the separatrix region of a magnetotail reconnection event.
345 *Geophysical Research Letters*, *46*(19), 10744–10753.
- 346 Zhou, M., Berchem, J., Walker, R., El-Alaoui, M., Goldstein, M., Lapenta, G., ...
347 others (2018). Magnetospheric multiscale observations of an ion diffusion
348 region with large guide field at the magnetopause: Current system, electron
349 heating, and plasma waves. *Journal of Geophysical Research: Space Physics*,
350 *123*(3), 1834–1852.